Characterization by NMR Spectroscopy of the SEI Layer Formed on Ti 3 C 2 MXene Materials Prepared with Various Terminations

Sanjay Sunny, Yannick Coppel, Pierre Louis Taberna, Patrice Simon

Journal of The
Electrochemical Society

Characterization by NMR Spectroscopy of the SEI Layer Formed on Ti_3C_2 MXene Materials Prepared with Various Terminations

Journal of The Electrochemical Society, 2024 **171** 030512

Characterization by NMR Spectroscopy of the SEI Layer Formed on Ti_3C_2 MXene Materials Prepared with Various Terminations

Sanjay Sunny,[1] Yannick Coppel,[2] Pierre Louis Taberna,[1,3,z] and Patrice Simon[1,3,z]

[1]*CIRIMAT, Université Toulouse 3 Paul Sabatier, Toulouse INP, CNRS, Universit´e de Toulouse, 118 Route de Narbonne, Cedex 9, Toulouse 31062, France*
[2]*CNRS, LCC (Laboratoire de Chimie de Coordination), Université de Toulouse, UPS, INPT, 205 route de Narbonne, BP 44099, F-31077 Toulouse Cedex 4, France*
[3]*ALISTORE-European Research Institute, France*

The nature and content of surface terminations are one of the key factors that define the electrochemical signature of the widely studied MXene materials. In this paper, the surface termination of molten salt synthesized $Ti_3C_2T_x$ MXene with -O and -Cl terminations (T=Cl,O) are studied for the first time using solid state NMR technique, with respect to conventional HF synthesized $Ti_3C_2T_x$ (T=F, O, OH). Both materials have been further used as negative electrode of Li-ion battery. The evolution of surface terminations during the Solid Electrolyte Interphase (SEI) layer formation was studied from the SEI components formed in both MXenes. Analysis of the NMR signal provided insights into the porous nature of SEI with LiF as main component in HF terminated MXenes. While a thick uniform formation of the SEI was observed for the molten salt synthesized $Ti_3C_2T_x$ (T=Cl,O) with Li_2CO_3 as dominant component.

 [DOI: 10.1149/1945-7111/ad2d1a]

Manuscript submitted December 30, 2023; revised manuscript received February 13, 2024. Published March 11, 2024.

Supplementary material for this article is available online

MXenes are two-dimensional transition metal carbides/nitrides with general chemical formulae of $M_{n+1}X_nT_x$ (M = transition metal, X = C/N, Tx = surface terminations).[1,2] Due to their inherent versatile properties, MXenes are envisioned in wide range of field like energy storage, coatings and composites, electromagnetic interference shielding, and the list extends to biomedical applications.[3–8] Tunable interlayer spacing, conductive metal carbide core and tunable surface terminations are a few among the properties that makes MXenes an active material of interest for energy storage applications.[9]

Diverse redox chemistries, achieved through surface terminations, have made Ti_3C_2 MXene, the most studied MXene, as a potential anode active material in lithium ion batteries.[10] Conventional synthesis of MXene includes a wet chemical etching of the "A" element, using fluoride containing salts, from the parent MAX phase.[11] Recently a new molten salt etching synthesis route was introduced opening new horizons regarding the nature of surface terminations and has reported to perform as better anode in Li-ion batteries.[12,13] The enhanced performance is attributed to the variation in the surface terminations and is backed by various theoretical and experimental studies.[14]

Surface termination characterization of the MXenes synthesized through various routes have been reported before: X-ray photoelectron spectroscopy (XPS),[15] Raman spectroscopy,[16,17] solid-state nuclear magnetic resonance (ssNMR),[18–21] Fourier transform infrared spectroscopy (FT-IR),[22,23] thermogravimetric analysis (TGA)[13,24] are few among the qualitative and quantitative techniques used for the characterizations. The characterization of the terminations has been difficult due to many reasons like variation in the probed volume, impurities present and the differences in intercalant species *etc* Only a few studies have been conducted with ssNMR and to the best of our knowledge all the studies were on wet chemically etched MXenes.[20,21,25–28]

While surface termination influences the electrochemical properties, modification of the same also happens during the cycling.[29] Moreover, those surface terminations have been reported to affect the solid electrolyte interphase (SEI) formation during the initial electrochemical cycles, as the electrolyte reduction mechanisms are dependent of its interplay with those surface terminations.[14] Overall, the type of the electrolyte used, cycling condition, amount of water content are few among the many factors that influence the amount and composition of the SEI formed. LiF, LiOH, Li_2CO_3, $ROCO_2Li$, ROLi and polyethylene oxides are the most common decomposition products of the LP30 (1 M $LiPF_6$ in EC:DMC) electrolyte, the commercially used Li-ion battery electrolyte.[30] A robust, thin, ionically conducting and electronically insulating SEI ensures better anode performance with longer cycle life and enhanced efficiency. Despite its significance, the composition of the components and the formation mechanism is still unclear. Variations in morphology and thickness (ranging from 1 to 100 nm) of SEI have been reported[31] and the variation is also observed in the MXenes.[32,33] Thus, the studies of SEI formed on MXenes with different surface terminations is of paramount importance to understand the charge storage mechanism and the ageing process.

Solid-state NMR (ssNMR) turns up being a relevant technique for such study. As a matter of fact, probing the chemical bonds is expected to grasp insights regarding the MXene's surface terminations and their interplay with the electrolyte giving rise to the SEI. Herein, it is proposed to compare SEI formation and change upon cycling of MXenes exhibiting different initial surface terminations: HF $Ti_3C_2T_x$ MXene and MS $Ti_3C_2T_x$ MXene. For this purpose, ^1H, ^{13}C and ^{19}F as nuclear probes have been used for the current work. The MXene materials were cycled in commercially used LP30 electrolyte with a hold at low potential. Thus, the nature of the formed solid electrolyte interphases depending on the surface terminations were studied using different ssNMR techniques.

Experimental Methods

Synthesis of $Ti_3C_2T_x$ (T=F, O, OH) MXene.—$Ti_3C_2T_x$ (T=F, O, OH) was synthesized from 1 g of commercially available Ti_3AlC_2 MAX powder as described elsewhere.[34] 20 ml of etching solution (6:3:1 vol % mixture of 12 M HCl:DI water:HF) was taken in 50 ml polyethylene container for the synthesis. The MAX was slowly added to the etching solution and stirred at 35 °C for 24 h with loosen cap (for gas evolution). The etched solution was centrifuged at 5000 rpm for 3 min multiple times with DI water till the pH was 5. The centrifuged material was further washed in DI water and vacuum filtered with cellulose filter. The multilayer powder thus obtained was dried in vacuum oven overnight at 80 °C.

[z]E-mail: pierre-louis.taberna@univ-tlse3.fr; patrice.simon@univ-tlse3.fr

Synthesis $Ti_3C_2T_x$ (T=Cl,O) MXene.—1 g of Ti_3AlC_2 MAX powder was used for the synthesis with $CuCl_2$ as the Lewis acid salt and NaCl & KCl as supporting salts (Ti_3AlC_2:$CuCl_2$:NaCl:KCl = 1:3:2:2 in molar ratio). The salts and the precursors were carefully weighed and stirred well in mortar to obtain homogeneous mixture. The mixture was further heated in a tube furnace with argon flow (ultrapure 5.0 99.99%) for 12 h at 700 °C to etch the aluminum. Once cooled down to room temperature, the product was washed in DI water to remove the excess salt followed by vacuum filtration. The filtered product was stirred in 0.1 M ammonium persulfate ($(NH_4)_2S_2O_8$, Sigma-Aldrich, CAS # 7727–54–0) solution for removing the copper impurities formed during synthesis. The solution was filtered and washed several times in DI water to remove the impurities subsequently dried in vacuum oven for 24 h at 80 °C.

Physical characterization.—X-ray diffraction analysis was performed using D-8 diffractometer (Endeavor, Bruker) with Cu-Kα radiation (40 kV, 25 mA) from 5°–80°. Morphology was analyzed using scanning electron microscopy (SEM-FEG, JSM-7900F) at 20 kV. Fourier transform infrared spectroscopy (FTIR was performed using Thermo Scientific Nicolet model 6700 FT-IR spectrometer between 4000 and 400 cm^{-1}. Raman spectra studies were conducted with Xplora (HORIBA company) equipment and the 785 nm laser was used for the excitation.

Electrochemical measurements.—All the electrochemical studies were performed in two-electrode coin cells (CR2032). The working electrode were prepared using slurry coating on copper foil using doctor blade. Pristine MXene powder, acetylene carbon black and polyvinylidene fluoride was taken in 80:10:10 ratio in N-Methyl-2-pyrrolidone solvent. Followed by overnight vacuum drying, 12 mm-diameter discs were cut from the electrode with an average mass loading of 6 mg cm^{-2}. The electrodes were cycled in 1 M $LiPF_6$ in ethylene carbonate- dimethyl carbonate (1:1 Vol%, 99.9% pure Solvonic) electrolyte with Li foil (Sigma-Aldrich, purity of 99.9%) as counter and Ref. 17 mm-diameter glass microfiber A (Whatman) was used as the separator and coin cells were assembled in argon filled glovebox (H_2O < 0.1 ppm and O_2 < 0.1 ppm).

Biologic VMP3 potentiostat was used for the electrochemical tests and all the studies were conducted at room temperature. Linear sweep voltammetry technique from OCV to 0.2 V (vs Li^+/Li) at 0.1 mV sec^{-1} scan rate was performed followed by a 15 min hold at 0.2 V for the formation of SEI. Further cyclic voltammetry at the same scan rate was conducted for 3 cycles to ensure the SEI formation. All the coin cells were dismantled at similar potentials (approx. 1.5–2 V) inside the argon filled glovebox. The working electrode material was scratched without any rinsing step and was dried in the glovebox for 2 d. A portion of the as dried material was further vacuum dried in 80 °C overnight for removing the excess electrolyte solvents.

Solid-state NMR measurements.—NMR experiments were recorded on a Bruker Avance 400 III HD spectrometer operating at magnetic fields of 9.4 T. Samples were packed into 3.2, 2.5 or 1.3 mm zirconia rotors and were rotated at frequencies between 14 and 50 kHz at 295 K. ^{1}H MAS were performed with the DEPTH pulse sequence and a recycle delay of 3 s. ^{1}H MAS with rotor synchronous dipolar filtering and spin echo excitation (DF-SE)[35] were acquired with a filtering time between 0.8 and 26.1 ms. ^{13}C Hahn-echo were recorded with a recycle time between 5 and 10 s and an echo time of 1 rotor period. ^{13}C CPMG were acquired with 20 echoes, a delay between train of 180° pulse of 5 rotor periods and a recycle delay of 2 s. ^{13}C CP MAS spectra were recorded with a recycle delay of 2 s and a contact time of 2 ms. ^{19}F MAS spectra were measured with a recycle delay of 2 s. Chemical shifts were externally referenced to liquid TMS and CCl_3F for ^{1}H, ^{13}Cand ^{19}F, respectively. The rotors were fully packed with the MXene samples before characterization. The average mass difference of MXene filled rotors was observed to be less than 12% from 5 trials of weighing.

Results

Hydrogen Fluoride and molten salt-based synthesis of $Ti_3C_2T_x$ MXenes were prepared from commercial Ti_3AlC_2 MAX phase powders from two different synthetic routes, such as detailed in experimental section. The first one is based on the etching of Al atoms by immersion of the MAX precursor in a mixture of HCl and HF aqueous electrolyte, resulting in mainly -F, and -OH terminated Ti_3C_2 MXenes, termed as HF-Ti_3C_2. In a second route, $Ti_3C_2T_x$ MXenes are prepared by etching MAX phase in a molten salt electrolyte, containing $CuCl_2$ as the etchant, resulting -Cl and -O terminated Ti_3C_2 MXenes termed as MS-Ti_3C_2. These termination differences have direct influence on surface chemistry, like reduced hydrophilicity, due to lack of -OH terminations. The latter synthesis route leads to oxidation of carbon during the ammonium persulfate (APS) wash.[13]

The successful etching of the MAX to MXene was confirmed from the scanning electron microscopy (SEM) images and 00 *l* peak

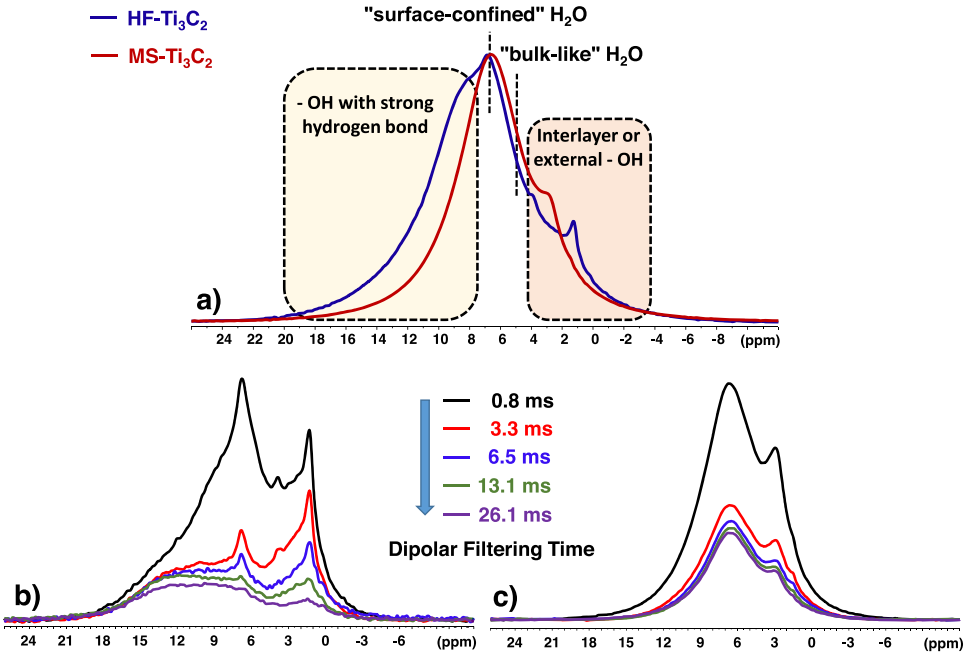

Figure 1. ^{1}H MAS of pristine powder (a)–(b) HF-Ti_3C_2 and (a)–(c) MS-Ti_3C_2, (a) without and (b)–(c) with dipolar filtering. For (a) signal intensities were normalized to the water signal around 6.5 ppm. (The expected position of the main types of water signals are given as a guide for the eyes).

shift to lower angles in X-ray Diffraction (XRD) (Figs. S1 and S2 respectively). The intense (002) peak shift from 9.56° to 8° for molten salt MXene and to 7.8° for the HF MXene. The shift to lower angle shows the expansion of interlayer after the etching process. A very small amount of unetched MAX can also be found for HF MXene resulting in additional peaks. Preliminary characterization of the pristine powder samples obtained were performed through Raman and FT-IR spectroscopy (Figs. S3 and S4 respectively). Apart from the characteristic main peaks, a clear difference in surface terminations were not observed from these spectra. The electrochemical cycling of the materials in commercial LP30 electrolyte produced signatures similar to that reported before (Fig. S5). The molten salt synthesized MXene (MS-Ti_3C_2) shows improved capacity at a lower average discharge potential vs HF-MXene, making it a better anode.[13]

Solid state NMR studies of surface terminations of pristine MXenes.—Figure 1 portraits the ^{1}H ssNMR spectra without or with dipolar filtering (DF-SE) obtained under fast magic angle spinning (MAS) for HF-Ti_3C_2 (Figs. 1a and 1b and MS-Ti_3C_2 (Figs. 1a and 1c) synthesized samples. Regarding ^{1}H MAS NMR spectra (Fig. 1a), MXenes show a broad ^{1}H signals at ∼6 ppm that represents a distribution of hydroxyl signals of water molecules including notably signals corresponding to "surface-confined" water at ∼6.7 ppm and "bulk-like" water at ∼5.0 ppm,[17] -OH terminations engaged in strong hydrogen bonds (7–15 ppm range) and -OH with weak hydrogen bonds (interlayer and external Ti-OH terminations) and/or intercalant contaminants[19,26] in the 0 to 4 ppm range.

The assignment of the 7–15 ppm area to hydroxyl group agrees with the previous reports where the broadness can be due to the variation in the hydrogen bonding strength.[20,26] The hydrogen bonding initiated through hydroxyl group was supported by MD simulation and experimental results.[24] Some previous studies have also assigned the peak in the 0–4 ppm range shift to the interlayer (within the multilayered structure) and external (on outer surface of multilayered structure) hydroxyl groups, which was also backed by Density Functional Theory (DFT) calculations.[21,27] The HF-Ti_3C_2 is expected to have more -OH terminations than MS-Ti_3C_2 due to their aqueous acid-based synthesis technique.[13] The amount and the relative proportion of water signals (between 4.5 and 7 ppm) is much greater for MS than for HF MXene (Fig. S6). For further information on the nature of H species, we performed ^{1}H MAS ssNMR with dipolar filtering experiments that enable signals to be edited according to the intensity of their dipolar couplings, by adjusting the length of the dipolar filter. The stronger the dipolar couplings, the faster the signals disappear with the dipolar filter. Rigid H atoms involved in multiple dipolar couplings with nearby H atoms will rapidly loss their intensity as filtration time increases. On the contrary, long filtration times can be used to highlight either H atoms with high local mobility (which reduce dipolar coupling strength) or isolated H atoms. For HF-Ti_3C_2 (Fig. 1b, a fast decrease of the signals of the surface water and -OH groups engaged in moderate hydrogen bonds (7–9 ppm range) is observed. By using the longest filtering times, we retain mainly the signals from isolated species, particularly those involved in very strong H-bonds (above 9 ppm) or interlayer Ti-OH terminations (around 1.5 ppm) for HF-Ti_3C_2. By comparison, all MS-Ti_3C_2 signals decrease in a similar way with the length of the dipole filters (Fig. 1c). Signal loss between the shortest and longest filter times is 80% and 68% for HF and MS MXene respectively. These results confirm a higher proportion of relatively mobile "bulk-like" water for MS MXene and a lower proportion of -OH terminations.

To go further, ^{13}C MAS NMR experiments for the HF and MS MXene powder were carried out (Fig. 2) showing significant differences. An asymmetric signal at ca 392 ppm was observed for the HF-Ti_3C_2, which is similar to shift reported in previous synthesis method.[20,26] In contrast for MS-Ti_3C_2, this ^{13}C signal was observed at a lower chemical shift of 362 ppm. This difference can be explained by the fact that ^{13}C shift has been shown to be quantitatively dependent on $Ti_3C_2T_x$ MXene surface functionalization (−O,−OH, −F, −Cl),[18] confirming the difference in their surface terminations. The signal broadness in turn, depends on homogeneity of the distribution of surface groups and the broader signal for the HF-Ti_3C_2 in comparison to MS-Ti_3C_2, might be due to the inhomogeneous and defective nature of HF MXene. Anisotropic bulk magnetic susceptibility linked to high anisotropy and local conductivity is another factor that could explain this peak broadness.[36,37]

Interestingly, additional peaks are also detected in the 0–200 ppm range. Some of these peaks are also observed with the cross polarization (CP) MAS experiment (Fig. 2c) which is based on dipolar magnetization transfer between hydrogen and carbon atoms. That signal region may be ascribed in part to the oxidation of carbon into carbonyl (200–150 ppm), CO_2 (130 ppm), acetal (100 ppm), alkane (0–50 ppm) groups during the APS wash achieved to remove Cu.[13,38] This finding is in line with previous temperature programmed desorption- mass spectroscopy (TPD-MS) studies showing carbon oxidation occurs upon persulfate wash, altering the carbon stoichiometry.[13] The modification of the chemical composition probably had an impact on the chemical shift of the ^{13}C MXene signal,[18] such as observed here for the MS in comparison to HF-Ti_3C_2.

To summarize, ssNMR analysis revealed clear differences in the surface terminations of MXenes synthesized through two different routes. Enhanced presence of hydroxyl terminations on HF-Ti_3C_2 and evidence of carbon oxidation on MS-Ti_3C_2 were observed. These surface termination differences can directly impact the electrochemical performance, especially in the formation of the solid electrolyte interphase. ssNMR was then utilized to explore the modification of the surface terminations during the SEI formation process.

Solid state NMR studies on SEI formed electrodes.—The solid electrolyte interphase was formed on the HF and MS MXene using slow scan rate (at 0.1 mV s^{-1}) cyclic voltammetry with potential hold, as mentioned in the experimental section. Briefly, the cells were cycled using linear sweep voltammetry at 0.1 mV sec^{-1} from OCV to 0.2 V (vs Li^+/Li) with a potential hold of 15 min at 0.2 V. Further, 3 cyclic voltammetry cycles were performed at the same scan rate to ensure the formation of SEI before dismantling inside a glove box. Samples were dried for 2 days inside the glovebox and used without any further washing to ensure that no dissolvable SEI components would be removed[30] - a portion of the recovered sample was dried further inside a vacuum oven at 80 °C for 12 h before analysis.

The samples were then first analyzed in ^{1}H MAS NMR, notably with a dipolar filter of 13 ms as presented in Figs. 3a, 3b for HF-MXene and MS-MXene, with and without the presence of SEI at the surface.

Significant differences are observed in the case of intensities of the ^{1}H signals for both the MXenes. A very strong and sharp peak at 4.2 ppm was observed for the HF-Ti_3C_2 post SEI formation (Fig. 3a); this peak can be attributed to the presence of trapped ethylene carbonate.[25,30] In addition, in situ XRD studies have shown that the c parameter of HF MXene was increased during Li intercalation, differently from MS. Such interlayer distance expansion for HF MXene, combined with the NMR results, could be linked to the intercalation of solvent molecules together with Li ions (solvated Li^+), finally trapping some solvent between the layers. The possibility of entrapment of solvent in porous SEI and the direct correlation of the peak intensity with the irreversible capacity loss during initial cycles of graphite anode was also suggested before.[30] Differently, the absence of a peak at 4.2 ppm for MS-Ti_3C_2 - SEI suggests the absence of solvent molecules in the SEI layer and between the layers of MXene. Additionally, main signals for MS-Ti_3C_2 post SEI formation are observed at 1.3 and 0.9 ppm (Fig. 3b). These peaks was assigned to CH_2 and CH_3 alkyl groups in the previous reports, which can be found in carbonate based SEI

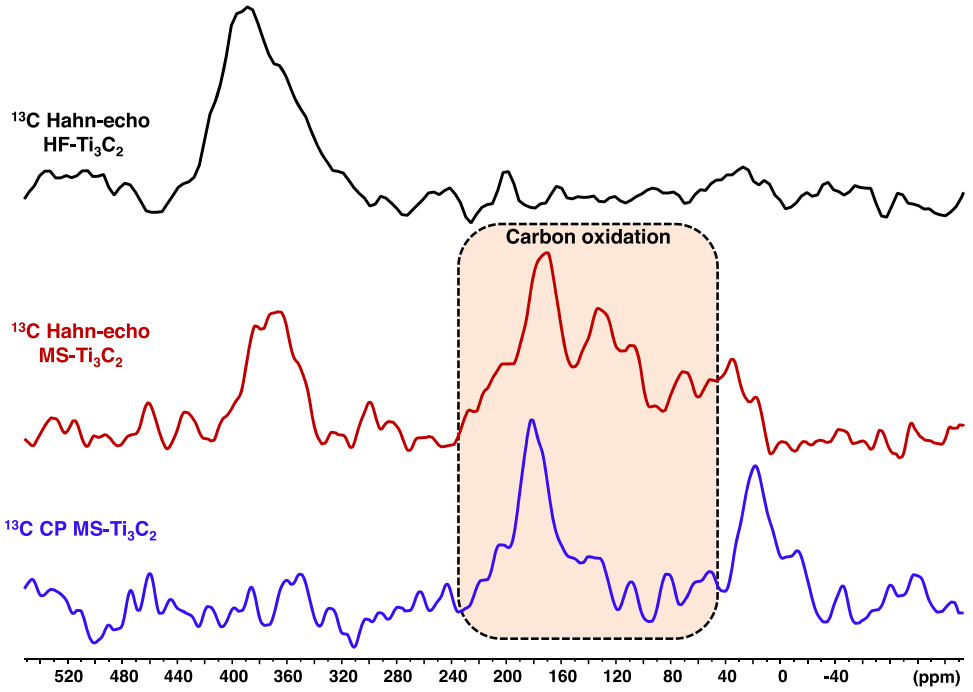

Figure 2. ^{13}C Hahn-echo and Cross polarization (CP) MAS of HF-Ti_3C_2 and MS-Ti_3C_2.

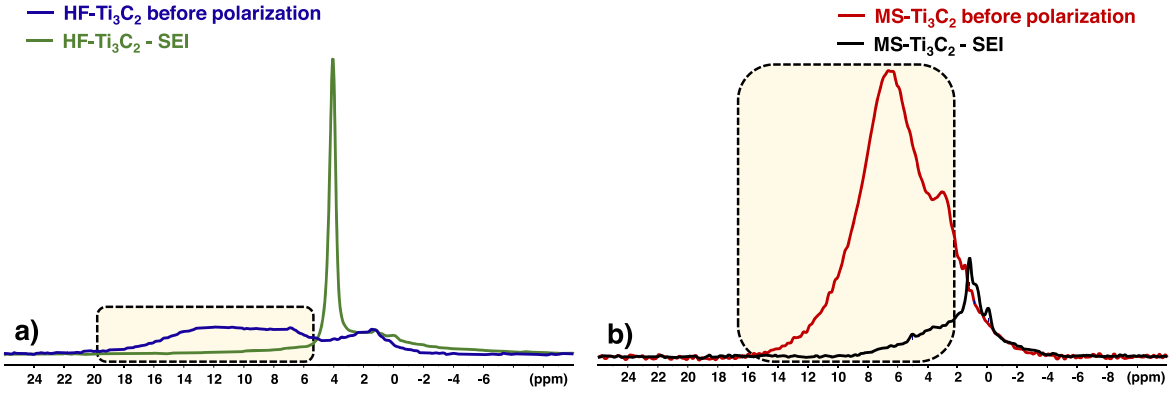

Figure 3. ^{1}H MAS ssNMR with a dipolar filter of 13 ms of pristine powder & SEI formed electrode (a) HF-Ti_3C_2 and (b) MS-Ti_3C_2. Signal intensities were normalized to the signal around 1.5 ppm corresponding to the Ti-OH terminations.

components.[30] Finally, a strong reduction in the signal intensity of water and -OH regions above 7 ppm (rectangular box) are evidenced for both MXenes. This was expected considering the instability of the water and -OH groups at high cathodic potential applied during the SEI formation. As the initial amount of water signal was more pronounced for MS-MXene, its strong reduction could be a reason for the high initial irreversible capacity. Although the presence of confined unreacted water cannot be definitively excluded, it seems unlikely considering the high cathodic potential applied during the electrochemical polarization. Thus, the post SEI HF-MXene shows the evidence of ethylene carbonate entrapment within the layers (suggested by the expansion of the interlayer distance) and possibly within the porous SEI, while the MS-MXene shows an reduction of water and -OH peaks with more alkyl decomposition products.[30]

To go further in the SEI analysis ^{13}C MAS NMR experiments were performed. The obtained spectra (Fig. 4a) shows a broad characteristic signal at ca 390 ppm for HF-Ti_3C_2 - SEI, which is similar to the pristine powder samples. Surprisingly, this signal was lost for the MS-Ti_3C_2 after SEI formation (Fig. 4b). ^{13}C NMR analyses were also performed with the Carr-Purcell-Meiboom-Gill (CPMG) protocol (Figs. 4c, 4d), which generally gives a much better noise-to-noise ratio for broad signals, as seen for HF-Ti_3C_2 - SEI. Again, no ^{13}C spikelet signals in the 300–400 ppm area could be observed for MS-Ti_3C_2 - SEI. The loss of this carbon signal can be potentially associated with a strong broadening of the resonance, originating from fast transverse (T_2) relaxation. This fast transverse relaxation may have several causes: (i) presence of more amorphous carbon (lithium alkyl carbonates) in the SEI,[39,40] (ii) magnetic anisotropies dependent on the surface terminations and defects,[41] (iii) post SEI carbon defects with local magnetic anisotropies,[42] and (iv) presence of paramagnetic radicals (alkoxide radicals) formed during the SEI or paramagnetic lithium in the SEI.[43,44] The broad set of signals observed between 0 and 200 ppm for both samples was assigned to carboxyl, carbonate and alkyl groups;[30] their amorphous nature leads to the broadness of these signals due to the distribution in the chemical shifts. This observation well agrees with the SEI layer formation on carbon, where the carboxyl/carbonate groups corresponds to the decomposition products of the electrolyte during the first cycle. Finally, a reduction of the electrical conductivity can be expected during the electrochemical cycling which can also act as a possible reason for the shift of the MXene signal (around 360 ppm) to lower ppm (<200 ppm).

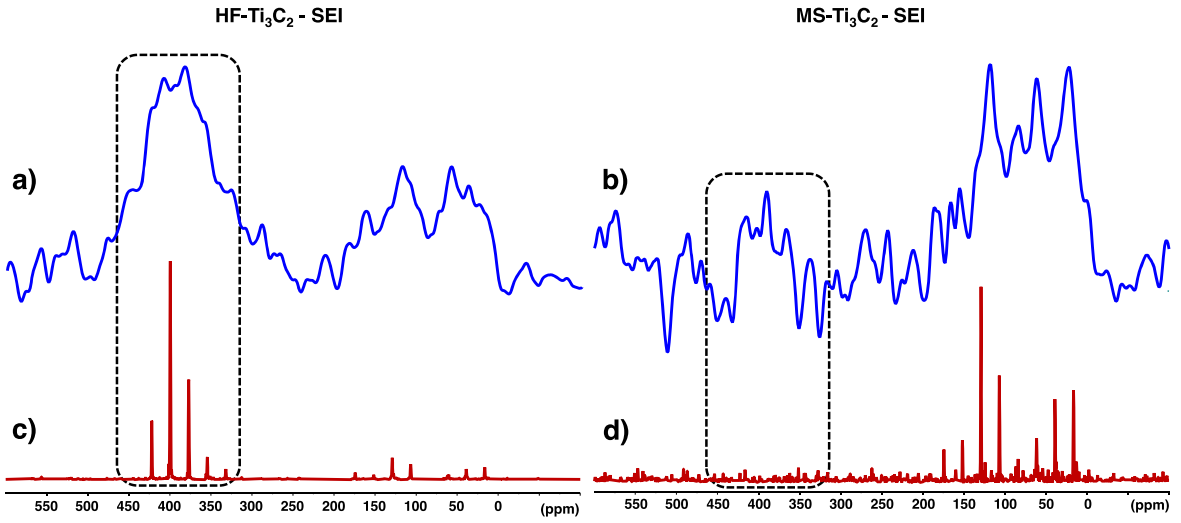

Figure 4. ^{13}C Hahn-echo (a), (b) and CPMG (c), (d) MAS of SEI formed HF-Ti_3C_2 (a), (c) and MS-Ti_3C_2 (b), (d).

^{19}F MAS characterization of HF pristine powder, HF and MS SEI formed electrodes were performed as shown in Figs. 5a and 5b respectively (pristine MS MXene does not contain any F terminations). Pristine powder samples (HF-Ti_3C_2) showed peaks corresponding to -F terminations on Ti (−246 ppm) and AlF_3 (−151 ppm), Al coming from MAX phase present as impurities. After SEI formation, both MS and HF MXene possess mainly three peaks corresponding to LiF (−200 ppm), $LiPF_6$ (−73 and −76 ppm) and PO_2F_2 (−93 and −99 ppm). The double signal observed at −170 and −182 ppm in Fig. 5b being close to the one observed for AlF_3 (Fig. 5b), these signals are assumed to be associated with Al species. The intensity of the LiF signal of HF-Ti_3C_2-SEI is far superior to that of MS counterpart, confirming the higher content of LiF in HF MXene. This strong signal arises at the expense of peak corresponding to -F terminations observed for the pristine sample at −246 ppm. It can be proposed that F terminations undergoes reaction during the SEI formation, resulting in the generation of fluorine and high amount of LiF. The higher LiF amount may also be due to ongoing electrolyte degradation, as LiF becomes one of the primary products of the first degradation of the LP30 electrolyte.

Discussion

ssNMR studies of the MXenes shows differences in the SEI components and surface termination modification during the process. Thus, the surface termination plays an important role in the SEI formation mechanism. The formation mechanism can depend on various factors and more studies are ongoing to get a deeper knowledge regarding the process. Here we propose SEI formation mechanism on two different MXenes based on the surface termination analysis, pre and post SEI formation, and the results are summarized in Fig. 6.

SEI formation on HF synthesized MXene.—According to previous studies on HF MXene, the abundant F terminations present are expected to generate LiF with high surface energy, which can lead to uniform SEI formation and fast Li ion diffusion. Besides, the SEI stability can likely benefit from the LiF being chemically stable and poorly soluble in the electrolyte - for those aforementioned advantageous properties, the use of F terminated MXenes as artificial SEI on metal anodes have been envisioned.[29,33] Nevertheless, an excessive amount of LiF has been reported to reduce the capacity of MXene and to affect the conductivity adversely.[14] Moreover, the uniformity of the SEI formed on HF MXene is questionable as previous studies on pristine F terminated MXenes have shown variations in the thickness and in the SEI components[32] and a possible dissolution for F terminated MXene has been also observed.[45,46] Herein, the outcome of this study shows the formation of high amount of LiF at the expense of F terminations in the SEI formed on HF MXene, (Fig. 5, ^{19}F ssNMR); a possible inhomogeneity in terminations, as indicated by the broadness of ^{13}C NMR of pristine powder (Fig. 2), might lead to the non-uniformity of the LiF. Moreover, further electrolyte decomposition can occur because of the presence of solvent within the SEI in contact with the surface. Those results tend to confirm that the SEI formed on HF-MXene is not stable.

SEI formation on MS synthesized MXene.—A high irreversible capacity loss and low coulombic efficiency for MS MXene is observed for the first cycle in comparison to HF. This irreversible

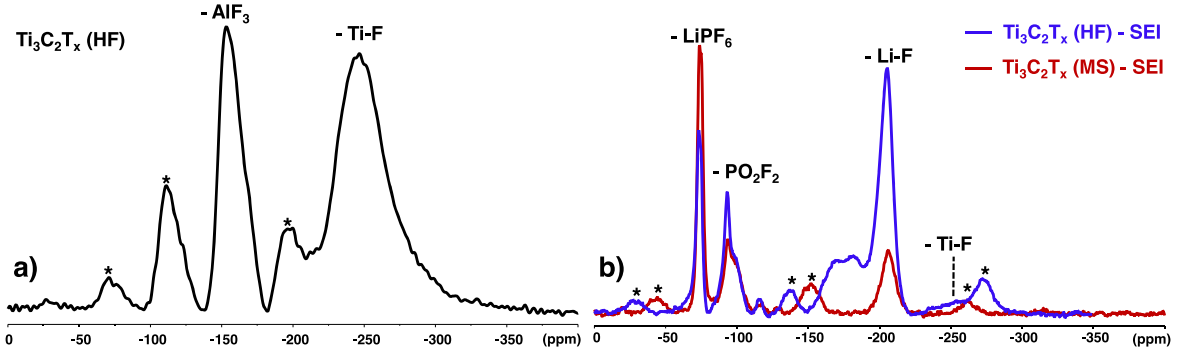

Figure 5. ^{19}F MAS of (a) Pristine HF-Ti_3C_2 powder (b) HF and MS-Ti_3C_2 SEI formed MXene. In (b) both spectrum were recorded under identical experimental conditions (rotor fully filled with MXene powders). *:spinning sidebands.

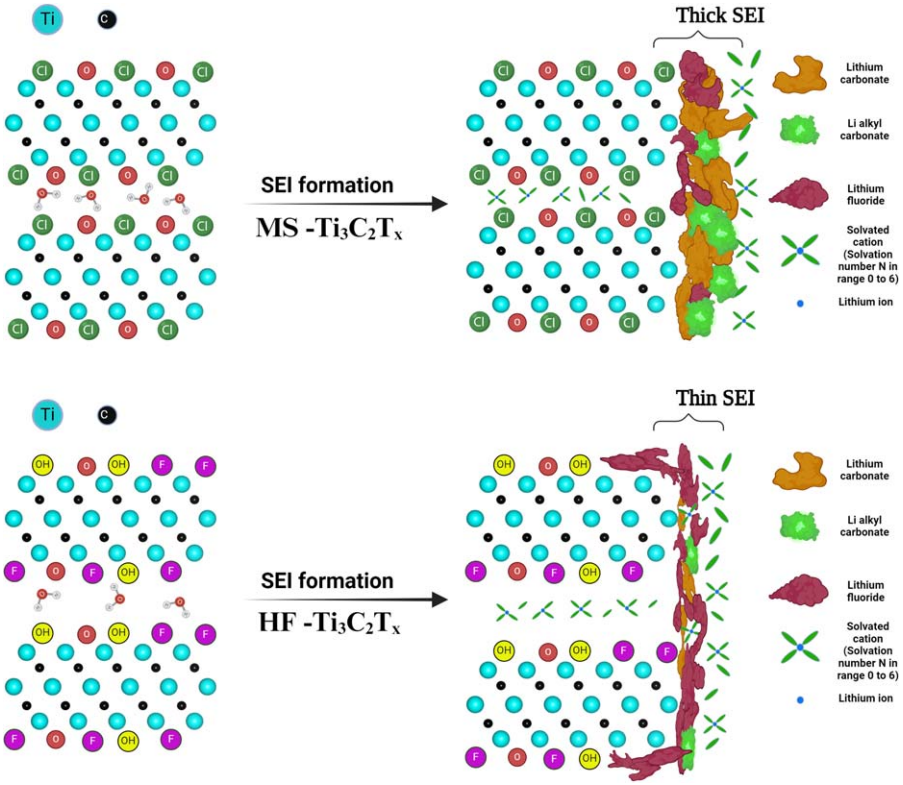

Figure 6. Schematic illustration of SEI formed on MXenes.

capacity can be correlated to a thicker SEI formed on the MS MXene. Adsorbed and intercalated water was suggested as one of the possible reasons for this irreversible capacity in HF MXene.[45] Similar percentage (5–7 wt%) of water was observed from TPD-MS studies conducted earlier on both the pristine MXenes. The ^{1}H spectra (Fig. 3) shows a pronounced water signal for MS pristine powder with an evident reduction of the same post SEI. Presence of water, either in electrolyte or in the material, has observed to react with other decomposition products to form inorganic components like Li_2CO_3.[31] Thus, presence of more Li_2CO_3 can be expected on MS MXene through similar reaction pathway.

Oxygenated functional groups on carbon-based anodes are assumed to be directly correlated to the initial capacity loss. Previous studies on graphene oxide attribute up to 70% of the initial irreversible capacity to surface oxygen and leading to the formation of COOLi from COOH and OLi.[47–49] As a result, a similar trend can be expected in the molten salt synthesized MXenes since oxygen terminations are formed on the carbon during APS washing.[13] Indeed, the present ^{13}C ssNMR studies on pristine MS powder shows additional peaks due to carbon oxidation. It is worth mentioning the nature of the O terminations also influences the SEI components formed: carbonyl groups react with electrolyte to form inorganic Li_2CO_3, while single bonded oxygen leads to organic lithium alkyl carbonates, which can eventually convert to Li_2CO_3.[50] A higher presence of alkyl groups was also observed in ^{1}H and ^{13}C spectra of MS MXene post SEI. Modification of HF MXene with Fe_2O_3 has shown to produce uniform SEI with Li_2CO_3 as the dominant component.[46] Post SEI formation FT-IR also shows peaks corresponding to Li_2CO_3 and the peaks are dominant for MS MXene in comparison to HF (Fig. S7). A schematic illustration of the SEI components formed is depicted in Fig. 6.

Conclusions

Surface termination of $Ti_3C_2T_x$ synthesized through two different routes were studied using the ssNMR technique. The HF based synthesis resulted in MXene with -F and more -OH terminations than molten salt synthesized MXene. The aqueous acid-based synthesis was concluded as the reason for this increased presence of terminations. Broad ^{13}C NMR signals suggests possibility of non-homogeneous distribution of F terminations for HF MXene. In the case of MS MXene, oxidation of the carbon species was observed which attributed to the ammonium persulfate washing. Solid electrolyte interface formation was performed and post SEI termination modification was analyzed. A reduction of the amount of water and hydroxyl groups was observed in both the MXenes which was expected during the SEI formation process. Presence of high amount of LiF at the expense of F terminations was deduced from the ssNMR analyses for HF synthesized MXenes, together with solvent entrapment within the multilayers and possibly in the porous SEI layer. Those results suggest that the SEI layer formed on HF-MXene is not stable as -F terminations surface is consumed. Differently, the presence of oxygen terminations and carbon oxidation resulted in more Li_2CO_3 and lithium alkyl carbonates for the MS MXene. The increased presence of alkyl group in ssNMR and Li_2CO_3 in FT-IR spectra confirms this enrichment for the MS MXene. The high initial irreversible capacity for MS MXene was correlated to the formation of a thick SEI with Li_2CO_3 as dominant component.

Overall, surface termination characterization of both the MXenes and its modification during SEI formation was studied. A thick and stable SEI with Li_2CO_3 as dominant component was observed for MS MXenes, while LiF was observed as dominant SEI component for HF-synthesized MXenes. These differences were caused by various factors like synthesis route, water content and the surface termination which plays the key role. This thick and stable SEI can be one of the causes for the better anode performance of MS MXene in comparison to HF MXene.

Acknowledgments

As a part of the DESTINY PhD programme, SS and all the authors acknowledge the funding from the European Union's Horizon2020 research and innovation program under the Marie Skłodowska-Curie Actions COFUND (Grant Agreement #945357). PS and PLT were supported by the ERC Synergy Grant MoMa-Stor #951513. The authors acknowledge Sébastien Moyano from CEMES for technical support regarding Raman spectroscopy.

Supporting Information

SEM, XRD, cyclic voltammetry and spectroscopies (Raman and FTIR) of HF and MS-Ti_3C_2 MXene are included in the supplementary information. FTIR of the MXenes post SEI also included.

ORCID

Patrice Simon https://orcid.org/0000-0002-0461-8268

References

1. B. Anasori, M. R. Lukatskaya, and Y. Gogotsi, *Nature Reviews Materials*, **2**, 1 (2017).
2. M. Naguib, M. Kurtoglu, V. Presser, J. Lu, J. Niu, M. Heon, L. Hultman, Y. Gogotsi, and M. W. Barsoum, *Two-Dimensional Nanocrystals Produced by Exfoliation of Ti(3)AlC(2).*, **23**, 4248 (2011).
3. T. Tang, "Flexible and flame-retarding phosphorylated MXene/polypropylene composites for efficient electromagnetic interference shielding." *J. Mater. Sci.*, **111**, 66 (2022).
4. Y.-Z. Zhang, Y. Wang, Q. Jiang, J. K. El-Demellawi, H. Kim, and H. N. Alshareef, "MXene printing and patterned coating for device applications." *Adv. Mater.*, **32**, 1908486 (2020).
5. L. Wang, J. Cheng, Y. Zou, W. Zheng, Y. Wang, Y. Liu, H. Zhang, D. Zhang, and X. Ji, "Current advances and future perspectives of MXene-based electromagnetic interference shielding materials." *Adv. Compos. Hybrid Mater.*, **6**, 172 (2023).
6. I. Amin, H. Brekel ven den, K. Nemani, E. Batyrev, A. Vooys de, H. Weijde van der, B. Anasori, and N. R. Shiju, "Ti3C2T x MXene polymer composites for anticorrosion: an overview and perspective." *ACS Appl. Mater. Interfaces*, **14**, 43749 (2022).
7. K. Huang, Z. Li, J. Lin, G. Han, and P. Huang, "Two-dimensional transition metal carbides and nitrides (MXenes) for biomedical applications." *Chem. Soc. Rev.*, **47**, 5109 (2018).
8. X. Li, Z. Huang, C. E. Shuck, G. Liang, Y. Gogotsi, and C. Zhi, "MXene chemistry, electrochemistry and energy storage applications." *Nat. Rev. Chem.*, **6**, 389 (2022).
9. A. VahidMohammadi, J. Rosen, and Y. Gogotsi, "The world of two-dimensional carbides and nitrides (MXenes)." *Science*, **372**, eabf1581 (2021).
10. X. Zhang, Z. Zhang, and Z. Zhou, "MXene-based materials for electrochemical energy storage." *J. Energy Chem.*, **27**, 73 (2018).
11. M. Alhabeb, K. Maleski, B. Anasori, P. Lelyukh, L. Clark, S. Sin, and Y. Gogotsi, "Guidelines for synthesis and processing of two-dimensional titanium carbide (Ti3C2Tx MXene)." *Chem. Mater.*, **29**, 7633 (2017).
12. Y. Gogotsi and Q. Huang, "MXenes: two-dimensional building blocks for future materials and devices." *ACS Nano*, **15**, 5775 (2021).
13. Y. Li, "A general lewis acidic etching route for preparing MXenes with enhanced electrochemical performance in non-aqueous electrolyte." *Nat. Mater.*, **19**, 571 (2020).
14. H. Xu, W. Zhu, F. Sun, H. Qi, J. Zou, R. Laine, and W. Ding, "Turning Trash into treasure: MXene with intrinsic LiF solid electrolyte interfaces performs better and better during battery cycling." *Adv. Mater. Technol.*, **6**, 2000882 (2021).
15. I. Persson, L.-Å. Näslund, J. Halim, M. W. Barsoum, V. Darakchieva, J. Palisaitis, J. Rosen, and P. O. Å. Persson, "On the organization and thermal behavior of functional groups on Ti3C2 MXene surfaces in." *Vacuum. 2D Mater.*, **5**, 015002 (2017).
16. A. A. Emerenciano, R. M. do Nascimento, A. P. C. Barbosa, K. Ran, W. A. Meulenberg, and J. Gonzalez-Julian, "Ti3C2 MXene membranes for gas separation: influence of heat treatment conditions on D-spacing and surface functionalization." *Membranes*, **12**, 1025 (2022).
17. A. Sarycheva and Y. Gogotsi, "Raman spectroscopy analysis of the structure and surface chemistry of Ti3C2T x MXene." *Chem. Mater.*, **32**, 3480 (2020).
18. F. Brette, D. Kourati, M. Paris, L. Loupias, S. Célérier, T. Cabioc'h, M. Deschamps, F. Boucher, and V. Mauchamp, "Assessing the surface chemistry of 2D transition metal carbides (MXenes): a combined experimental/theoretical 13C solid state NMR approach." *J. Am. Chem. Soc.*, **145**, 4003 (2023).
19. K. J. Griffith, M. A. Hope, P. J. Reeves, M. Anayee, Y. Gogotsi, and C. P. Grey, "Bulk and surface chemistry of the niobium MAX and MXene phases from multinuclear solid-state NMR spectroscopy." *J. Am. Chem. Soc.*, **142**, 18924 (2020).
20. M. A. Hope, A. C. Forse, K. J. Griffith, M. R. Lukatskaya, M. Ghidiu, Y. Gogotsi, and C. P. Grey, *NMR Reveals the Surface Functionalisation of Ti3C2 MXene.*, **18**, 5099 (2016).
21. T. Kobayashi, Y. Sun, K. Prenger, D. Jiang, M. Naguib, and M. Pruski, "Nature of terminating hydroxyl groups and intercalating water in Ti3C2Tx MXenes: a study by 1H solid-state NMR and DFT calculations." *J. Phys. Chem. C*, **124**, 13649 (2020).
22. A. Qian, Y. Pang, G. Wang, Y. Hao, Y. Liu, H. Shi, C.-H. Chung, Z. Du, and F. Cheng, "Pseudocapacitive charge storage in MXene–V2O5 for asymmetric flexible energy storage devices." *ACS Appl. Mater. Interfaces*, **12**, 54791 (2020).
23. A. Qian, J. Y. Seo, H. Shi, J. Y. Lee, and C. Chung, "Surface functional groups and electrochemical behavior in dimethyl sulfoxide-delaminated Ti3C2Tx MXene." *Chem. Sus. Chem*, **11**, 3719 (2018).
24. H. Shao et al., *ACS Energy Letters*, **5**, 2873 (2020).
25. J. M. Griffin, A. C. Forse, W.-Y. Tsai, P.-L. Taberna, P. Simon, and C. P. Grey, "In situ NMR and electrochemical quartz crystal microbalance techniques reveal the structure of the electrical double layer in supercapacitors." *Nat. Mater.*, **14**, 812 (2015).
26. M. Anayee, N. Kurra, M. Alhabeb, M. Seredych, M. N. Hedhili, A-H. Emwas, H. N. Alshareef, B. Anasori, and Y. Gogotsi, *Chemical Communications*, **56**, 6090 (2020).
27. A. Sugahara, Y. Ando, S. Kajiyama, K. Yazawa, K. Gotoh, M. Otani, M. Okubo, and A. Yamada, "Negative dielectric constant of water confined in nanosheets." *Nat. Commun.*, **10**, 850 (2019).
28. W. Sun et al., "Multiscale and multimodal characterization of 2D titanium carbonitride MXene." *Adv. Mater. Interfaces*, **7**, 1902207 (2020).
29. F. Zhao, P. Zhai, Y. Wei, Z. Yang, Q. Chen, J. Zuo, X. Gu, and Y. Gong, "Constructing artificial SEI layer on lithiophilic MXene surface for high-performance lithium metal anodes." *Adv. Sci.*, **9**, 2103930 (2022).
30. A. L. Michan, M. Leskes, and C. P. Grey, "Voltage dependent solid electrolyte interphase formation in silicon electrodes: monitoring the formation of organic decomposition products." *Chem. Mater.*, **28**, 385 (2016).
31. P. G. Kitz, P. Novák, and E. J. Berg, "Influence of water contamination on the SEI formation in Li-ion cells: an operando EQCM-D study." *ACS Applied Materials & Interfaces*, **12**, 15934 (2020).
32. Y. Yan, X. Zhao, H. Dou, J. Wei, Z. Sun, Y.-S. He, Q. Dong, H. Xu, and X. Yang, "MXene frameworks promote the growth and stability of LiF-rich solid–electrolyte interphases on silicon nanoparticle bundles." *ACS Appl. Mater. Interfaces*, **12**, 18541 (2020).
33. D. Zhang, S. Wang, B. Li, Y. Gong, and S. Yang, "Horizontal growth of lithium on parallelly aligned MXene layers towards dendrite-free metallic lithium anodes." *Adv. Mater.*, **31**, 1901820 (2019).
34. T. S. Mathis, K. Maleski, A. Goad, A. Sarycheva, M. Anayee, A. C. Foucher, K. Hantanasirisakul, C. E. Shuck, E. A. Stach, and Y. Gogotsi, "Modified MAX phase synthesis for environmentally stable and highly conductive Ti3C2 MXene." *ACS Nano*, **15**, 6420 (2021).
35. A. S. Andreev and V. Livadaris, "Characterization of catalytic materials through a facile approach to probe OH groups by solid-state NMR." *J. Phys. Chem. C*, **121**, 14108 (2017).
36. D. L. Vanderhart, W. L. Earl, and A. N. Garroway, "Resolution in 13C NMR of organic solids using high-power proton decoupling and magic-angle sample spinning." *J. Magn. Reson. 1969*, **44**, 361 (1981).
37. R. Pigliapochi, L. O'Brien, A. J. Pell, M. W. Gaultois, Y. Janssen, P. G. Khalifah, and C. P. Grey, "When do anisotropic magnetic susceptibilities lead to large NMR shifts? exploring particle shape effects in the battery electrode material $LiFePO_4$." *J. Am. Chem. Soc.*, **141**, 13089 (2019).
38. L. Liu, H. Zschiesche, M. Antonietti, M. Gibilaro, P. Chamelot, L. Massot, P. Rozier, P.-L. Taberna, and P. Simon, "In situ synthesis of MXene with tunable morphology by electrochemical etching of MAX phase prepared in molten salt." *Adv. Energy Mater.*, **13**, 2203805 (2023).
39. J. LaManna, J. Braddock-Wilking, S.-H. Lin, and B. Feldman, "13C NMR spectroscopy of amorphous hydrogenated carbon nitride." *Solid State Commun.*, **109**, 573 (1999).
40. O. Borodin, G. D. Smith, and P. Fan, "Molecular dynamics simulations of lithium alkyl carbonates." *J. Phys. Chem. B*, **110**, 22773 (2006).
41. K. Zhang, M. Di, L. Fu, Y. Deng, Y. Du, and N. Tang, "Enhancing the magnetism of 2D carbide MXene Ti3C2Tx by H2 annealing." *Carbon*, **157**, 90 (2020).
42. J. C. C. Freitas, F. G. Emmerich, G. R. C. Cernicchiaro, L. C. Sampaio, and T. J. Bonagamba, "Magnetic susceptibility effects on 13C MAS NMR spectra of carbon materials and graphite." *Solid State Nucl. Magn. Reson.*, **20**, 61 (2001).
43. F. A. Soto, Y. Ma, J. M. Martinez de la Hoz, J. M. Seminario, and P. B. Balbuena, "Formation and growth mechanisms of solid-electrolyte interphase layers in rechargeable batteries." *Chem. Mater.*, **27**, 7990 (2015).
44. O. Schirmer, "The structure of the paramagnetic lithium center in zinc oxide and beryllium oxide." *J. Phys. Chem. Solids*, **29**, 1407 (1968).
45. T. Koriukina, A. Kotronia, J. Halim, M. Hahlin, J. Rosen, K. Edström, and L. Nyholm, "On the use of Ti_3C_2 T_x MXene as a negative electrode material for lithium-ion batteries." *ACS Omega*, **7**, 41696 (2022).
46. N. Zhao, Y. Yang, Y. Xiao, C. Wang, M. N. Ha, W. Cui, and X. Wang, "Unveiling the SEI layer formed on pillar-structured MXene anode towards enhanced li-ion storage." *Scr. Mater.*, **202**, 113988 (2021).
47. W. Xing and J. R. Dahn, "Study of irreversible capacities for Li insertion in hard and graphitic carbons." *J. Electrochem. Soc.*, **144**, 1195 (1997).
48. I. Obraztsov, A. Bakandritsos, V. Šedajová, R. Langer, P. Jakubec, G. Zoppellaro, M. Pykal, V. Presser, M. Otyepka, and R. Zbořil, "Graphene acid for lithium-ion batteries—carboxylation boosts storage capacity in graphene." *Adv. Energy Mater.*, **12**, 2103010 (2022).
49. E. Frackowiak and F. Beguin, "Electrochemical storage of energy in carbon nanotubes and nanostructured carbons." *Carbon*, **40**, 1775 (2002).
50. Y. Peng, Z. Chen, R. Zhang, W. Zhou, P. Gao, J. Wu, H. Liu, J. Liu, A. Hu, and X. Chen, "Oxygen-containing functional groups regulating the carbon/electrolyte interfacial properties toward enhanced K+ storage." *Nano-Micro Lett.*, **13**, 192 (2021).